

Two-stage WECC Composite Load Modeling: A Double Deep Q-Learning Networks Approach

Xinan Wang, *Student Member, IEEE*, Yishen Wang, *Member, IEEE*, Di Shi, *Senior Member, IEEE*, Jianhui Wang, *Senior Member, IEEE*, Zhiwei Wang, *Senior Member, IEEE*

Abstract—With the increasing complexity of modern power systems, conventional dynamic load modeling with ZIP and induction motors (ZIP + IM) is no longer adequate to address the current load characteristic transitions. In recent years, the WECC composite load model (WECC CLM) has shown to effectively capture the dynamic load responses over traditional load models in various stability studies and contingency analyses. However, a detailed WECC CLM model typically has a high degree of complexity, with over one hundred parameters, and no systematic approach to identifying and calibrating these parameters. Enabled by the wide deployment of PMUs and advanced deep learning algorithms, proposed here is a double deep Q-learning network (DDQN)-based, two-stage load modeling framework for the WECC CLM. This two-stage method decomposes the complicated WECC CLM for more efficient identification and does not require explicit model details. In the first stage, the DDQN agent determines an accurate load composition. In the second stage, the parameters of the WECC CLM are selected from a group of Monte-Carlo simulations. The set of selected load parameters is expected to best approximate the true transient responses. The proposed framework is verified using an IEEE 39-bus test system on commercial simulation platforms.

Index Terms—Load modeling, double deep Q-learning network, load component identification, measurement-based.

I. INTRODUCTION

Accurate dynamic load modeling is critical for power system transient stability analysis and various simulation-based studies [1]-[2]. It is also known to improve the power system operation flexibility, reduce system operating costs, and better determine the corridor transfer limits [3]-[4]. In the past few decades, both industry and academic researchers have widely used ZIP and induction motors (ZIP + IM) as the composite load model (CLM) for quantifying load characteristics [5]-[7], in which ZIP approximates the static load transient behaviors and the IM approximates the dynamic load transient behaviors. This ZIP + IM load model has shown to be effective for simulating many dynamics in the power systems, but in recent years, industry has started to observe various new load components, including single-phase IM, distributed energy resources (DER), and loads interfaced via power electronics that are being increasingly integrated into the system. The high penetration of these new types of loads brings profound changes to the transient characteristics at the load end,

which raises the necessity for more advanced load modeling. For example, the well-known fault-induced, delayed-voltage-recovery (FIDVR) event is caused by the stalling of low-inertia single-phase IMs [8] when the fault voltage is lower than their stall thresholds. An FIDVR event poses potentially voltage control losses and cascading failures in the power system [9]; however, FIDVR cannot be modeled by a conventional CLM model. Given these conditions, the WECC composite load model (WECC CLM) is proposed.

To date, WECC CLM is available from multiple commercial simulation tools such as the DSATools™, GE PSLF, and PowerWorld Simulator. However, the detailed model structure, control logic, and parameter settings of the WECC CLM are limited by software vendors, and thus not transparent to the public [12], which impacts WECC CLM's general adoption and practicality. Furthermore, lack of detailed open-source information about the WECC CLM presents another major roadblock for conducting load modeling and parameter identification studies for system stability analysis.

Current WECC CLM works can be classified into two groups, which are component-based methods that rely on load surveys [13], [14] and measurement-based numerical fitting methods [15], [17]. In [13] and [14], the WECC CLM's parameters are estimated from surveys of different customer classes and load type statistics. However, the granularity and accuracy of the survey data depend entirely on the survey agency, and there are many assumptions being made that cannot be definitively verified. In addition, the survey is generally not up to date and does not reflect real-time conditions. In practice, all these limitations bring challenges in modeling the actual dynamic responses.

In another approach, authors in [15] and [17] numerically solve the parameter fitting problem using nonlinear least squares estimators. In these methods, the parameter identifiability assessment and dimension reduction are conducted through sensitivity and dependency analyses. Though sensitivity analysis reflects the impacts of the individual parameter on the load dynamics, it fails to capture the mutual dependency between two or more parameters, which has been proved to be of great importance in composite load dynamics [16]. In [17], the authors define the parameter dependency as the similarity of their influences on the dynamic response trajectory. Such a dependency analysis still falls short in factoring in the impact of multiple parameters on the load transient dynamics at the same time. In fact, with over one hundred parameters in the WECC CLM, the true interactions among them are hard to fully assess.

This work is funded by SGCC Science and Technology Program under contract no. SGSDYT00FCJS1700676. X. Wang, Y. Wang, D. Shi and Z. Wang are with GEIRI North America, San Jose, CA 95134, USA. X. Wang and J. Wang are with the Department of Electrical and Computer Engineering, Southern Methodist University, Dallas, TX 75205 USA.

This paper proposes a double deep Q-learning network (DDQN)-based load modeling framework that can conduct load modeling on the WECC CLM without prior load survey information. As such it is different from most nonlinear least square estimator-based load modeling work. The model recasts the load modeling for the WECC CLM into a two-stage learning problem. In the first stage, a DDQN agent is trained to find a load composition ratio that is most likely to represent the true load fractions at the interesting bus. Then, in the second stage, Monte-Carlo simulations are conducted to select the load parameters for the load components. From the Monte-Carlo simulations, the one set of parameters that best approximates the true dynamic responses is chosen for the load model. The specification [18] of the WECC CLM indicates that each load component in the model represents the aggregation of a specific type of load. Under such a composite load structure, it has been observed in [19] and [21] that different load composition ratios could have very similar transient dynamics. Therefore, solving the load composition ratio first and conducting the load parameter identification based on the identified ratio can significantly reduce the problem's complexity and increase load parameter identification computational efficiency. Our proposed method offers the following unique features and contributions:

- 1) *A load modeling framework for the WECC CLM with limited prior knowledge to model details.* Only the dynamic response curve is required to implement the proposed learning framework.
- 2) *The load model identified by this framework is robust to various contingencies.* The fitted load model is verified to be effective to recover the true dynamics with different fault locations and different fault types.
- 3) *The proposed method is scalable to different composite load structures:* In the DDQN training environment, the action taken by the agent is designed to be the load fraction changes on different load types. This set up allows the proposed method to be scaled from conventional CLM load models such as ZIP + IM to larger load models like the WECC CLM. The method can be easily extended to load models with more load components like DERs.

The remainder of this paper is organized as follows. Section II discusses the load component definition in the WECC CLM and the associated parameter selection range of each component. Section III introduces the DDQN training environment formulation and the customized reward function. Section IV presents the case studies to validate the effectiveness of the proposed method using the DSATools™. Section V provides concluding remarks, discussions on future research.

II. WECC CLM INTRODUCTION

A. WECC CLM Structure

The WECC CLM is widely recognized as the state-of-the-art load model [10] due its robustness in modeling a variety of load compositions and its capability of simulating the electrical distance between the end-users and the transmission substations

[9].

The detailed load structure for the WECC CLM is shown in Fig. 1, which mainly consists of three parts: substation, feeder, and load. The parameters for substation and feeder parts, such as the substation shunt capacitance B_{SS} and transformer tap settings [11] usually follow the industry convention and do not have significant variance [20]-[22]. Therefore, in this paper, we set the feeder and substation parameters following industrial standard values [20]. The load in WECC CLM includes three three-phase induction motors, one single-phase induction motors, one electronic load, and one ZIP static load. Our load modeling work focuses on the load composition and parameter identification for these load components.

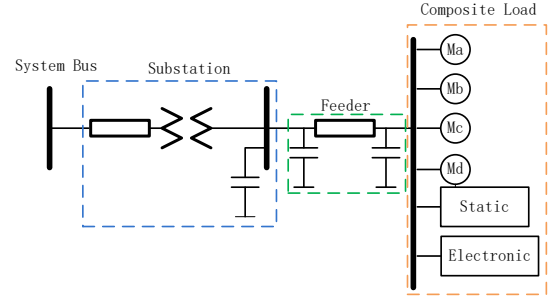


Fig. 1. WECC CLM structure [18]

B. Three-phase Induction Motors

As shown in Fig 1, four motors are connected at the end-use bus. Three of them are three-phase induction motors, which are defined as Ma , Mb , and Mc in our system setup. Ma , Mb and Mc use the same fifth-order induction motor model shown from (1) - (9), which are derived from the three-phase motor model block diagram given by WECC [18]:

$$\frac{dE'_q}{dt} = -\frac{1}{T_{po}} [E'_q + (L_s - L_p)i_d] - \omega_0 \cdot s \cdot E'_d, \quad (1)$$

$$\frac{dE'_d}{dt} = -\frac{1}{T_{po}} [E'_d - (L_s - L_p)i_q] + \omega_0 \cdot s \cdot E'_q, \quad (2)$$

$$\begin{aligned} \frac{dE''_q}{dt} = & \left(\frac{1}{T_{ppo}} - \frac{1}{T_{po}} \right) E'_q - \left(\frac{L_s - L_p}{T_{po}} + \frac{L_p - L_{pp}}{T_{ppo}} \right) i_d + \omega_0 \cdot s \cdot \\ & (1 - T_{po}) \cdot E'_d - \frac{1}{T_{ppo}} E''_q - \omega_0 \cdot s \cdot E''_d, \end{aligned} \quad (3)$$

$$\begin{aligned} \frac{dE''_d}{dt} = & \left(\frac{1}{T_{ppo}} - \frac{1}{T_{po}} \right) E'_d + \left(\frac{L_s - L_p}{T_{po}} + \frac{L_p - L_{pp}}{T_{ppo}} \right) i_q - \omega_0 \cdot s \cdot \\ & (1 - T_{po}) \cdot E'_q - \frac{1}{T_{ppo}} E''_d + \omega_0 \cdot s \cdot E''_q, \end{aligned} \quad (4)$$

$$\frac{ds}{dt} = -\frac{E''_d i_d + E''_q i_q - T_{mo} \omega_0^{Etrq}}{2H}, \quad (5)$$

$$i_d = \frac{R_s(V_d - E''_d) + L_{pp}(V_q - E''_q)}{R_s^2 + L_{pp}^2}, \quad (6)$$

$$i_q = \frac{R_s(V_q - E''_q) - L_{pp}(V_d - E''_d)}{R_s^2 + L_{pp}^2}, \quad (7)$$

$$p_{3\phi} = \frac{[R_s(V_d^2 + V_q^2 - V_d E''_d - V_q E''_q) - L_{pp}(V_d E''_q - V_q E''_d)]}{R_s^2 + L_{pp}^2}, \quad (8)$$

$$q_{3\phi} = \frac{L_{pp}(V_d^2 + V_q^2 - V_d E''_d - V_q E''_q) - R_s(V_d E''_q - V_q E''_d)}{R_s^2 + L_{pp}^2}. \quad (9)$$

where E_q' and E_d' are the transient voltages for IM on q-axis and d-axis. E_q'' and E_d'' represent the sub-transient voltages for IM on q-axis and d-axis. T_{p0} and T_{pp0} refer to the transient open-circuit time constant. L_s , L_p , and L_{pp} indicate the synchronous reactance, transient reactance, and sub-transient reactance. Stator resistance is denoted by R_s .

Each of the three-phase induction motors represents a specific type of dynamic load. According to [20], **Ma** indicates the aggregation of the three-phase motor's driving constant torque loads, such as commercial/industrial air conditioner; **Mb** represents the aggregation of the three-phase motor's driving torque speed-squared loads with high inertia, such as fan motors used in residential and commercial buildings; **Mc** refers to the aggregation of three-phase motor's driving torque speed-squared loads with low inertia, such as direct-connected pump motors used in commercial buildings. Several technical reports [20], [22] have published their parameter settings for WECC CLM. However, those suggested parameters cannot accurately adapt and approximate every real-world case. Therefore, we design a variation range for each parameter based on [20] and assume the true values of these load parameters should fall into this range. Table I presents part of the designed parameter variation range for **Ma**, **Mb**, and **Mc**. In the first stage of our load modeling framework, which is the load composition identification, the load parameters of each load component are unknown and randomly selected from the designed range.

Parameter	Ma	Mb	Mc
R_s	[0.03, 0.05]	[0.03, 0.05]	[0.03, 0.05]
L_s	[1.50, 2.00]	[1.50, 2.00]	[1.50, 2.00]
L_p	[0.10, 0.15]	[0.17, 0.22]	[0.17, 0.22]
L_{pp}	[0.10, 0.20]	[0.12, 0.15]	[0.12, 0.15]
T_{p0}	[0.09, 0.10]	[0.18, 0.22]	[0.18, 0.22]
T_{pp0}	[1e-3, 2e-3]	[2e-3, 3e-3]	[2e-3, 3e-3]
H	[0.10, 0.20]	[0.25, 1.00]	[0.10, 0.20]

C. Single-phase Induction Motor

The single-phase IM **Md** is developed based on extensive laboratory testing by WECC [18], which can model both the protective devices and the compressors. The motor's P and Q consumptions are modeled with exponential characteristics, which are divided into three states as functions of bus voltage. State 1 applies when the bus voltage is higher than the motor compressor breakdown voltage (p.u.): $V > V_{brk}$, as shown in (10) state 2 applies when the bus voltage is in between the motor compressor breakdown voltage and motor compressor stall voltage: $V_{stall} \leq V \leq V_{brk}$, which is shown in (11); and state 3 applies when the bus voltage is lower than the motor compressor stall voltage: $V < V_{stall}$, as shown in (12):

$$state\ 1: \begin{cases} p_{1\phi} = p_{0,zip} \\ q_{1\phi} = q_{0,1\phi} + 6 \cdot (V - V_{brk})^2, \end{cases} \quad (10)$$

$$state\ 2: \begin{cases} p_{1\phi} = p_{0,1\phi} + 12 \cdot (V_{brk} - V)^{3.2} \\ q_{1\phi} = q_{0,1\phi} + 11 \cdot (V_{brk} - V)^{2.5}, \end{cases} \quad (11)$$

$$state\ 3: \begin{cases} p_{1\phi} = \frac{V^2}{R_{stall}} \\ q_{1\phi} = -\frac{V^2}{X_{stall}} \end{cases}. \quad (12)$$

where $p_{0,1\phi}$ and $q_{0,1\phi}$ are initial active and reactive power consumed by the single-phase motor. R_{stall} and X_{stall} are the compressor stalling resistance and reactance, respectively. The compressor motors are classified into two categories depending on if they can restart or not after stalling. The active power $p_{1\phi}$ and reactive power $q_{1\phi}$ consumed by all the compressor motors before and after stalling are shown in (13) and (14). A denotes the compressor motors that can be restarted, and B marks those that cannot be restarted. In (13), F_{rst} refers to the ratio between motor loads that can restart and the total motor loads. In (14), V_{rst} refers to the restarting voltage threshold for the stalled motors. $f(V > V_{rst})$ is the function of the P, Q recovery rate of the compressor motors that can be restarted.

$$before\ stalling: \begin{cases} p_A = p_{1\phi} * F_{rst} \\ q_A = q_{1\phi} * F_{rst} \end{cases}, \quad (13)$$

$$after\ stalling: \begin{cases} p_{1\phi} = p_A \cdot f(V > V_{rst}) + p_{B,stall} \\ q_{1\phi} = q_A \cdot f(V > V_{rst}) + q_{B,stall} \end{cases}. \quad (14)$$

Other than the voltage stalling feature introduced here, WECC CLM also incorporates a thermal relay feature into the single-phase motor, and the detailed information can be found in [18]. **Md**'s compressor dynamic model is the same as the three-phase IM as **Ma**, **Mb**, and **Mc**. We design the parameter selection range for **Md** according to [20]. The values of some critical parameters such as V_{stall} , V_{rst} , V_{brk} , and F_{rst} are selected from the ranges shown in Table II.

Parameter	V_{brk}	V_{rst}	V_{stall}	F_{rst}
	[0.85, 0.90]	[0.92, 0.96]	[0.75, 0.80]	[0.15, 0.30]

D. Static Load Model: ZIP

The standard ZIP model is used in WECC CLM to represent the static load. The corresponding active and reactive power are written in (15)-(17):

$$p_{zip} = p_{0,zip} \cdot \left(p_{1c} \cdot \left(\frac{V}{V_0} \right)^2 + p_{2c} \cdot \frac{V}{V_0} + p_{3c} \right), \quad (15)$$

$$q_{zip} = q_{0,zip} \cdot \left(q_{1c} \cdot \left(\frac{V}{V_0} \right)^2 + q_{2c} \cdot \frac{V}{V_0} + q_{3c} \right), \quad (16)$$

$$\begin{cases} p_{1c} + p_{2c} + p_{3c} = 1, (0 \leq p_{1c}, p_{2c}, p_{3c} \leq 1) \\ q_{1c} + q_{2c} + q_{3c} = 1, (0 \leq q_{1c}, q_{2c}, q_{3c} \leq 1) \end{cases}. \quad (17)$$

where, $p_{0,zip}$ and $q_{0,zip}$ are the initial active and reactive power consumed by the ZIP load. p_{1c} , p_{2c} , and p_{3c} are the coefficients for the active power of constant impedance, constant current, and constant power load. q_{1c} , q_{2c} , and q_{3c} are the coefficients for reactive power of constant impedance, constant current, and constant power load. To model the diversity of ZIP load, the $p_{1c,2c,3c}$ and $q_{1c,2c,3c}$ are set to be random within the boundary shown in (17).

E. Electronic Load

The electronic load model in the WECC CLM aims to simulate the linear load tripping phenomenon of electronics. It is modeled as a conditional linear function of the bus voltage V , as shown from the (18)-(19). V_{d1} represents the voltage threshold at which the electronic load starts to trip, V_{d2} indicates the voltage threshold at which all the electronic load trips, V_{min} tracks the minimum bus voltage during the transient, pf_{elc} denotes the power factor of electronic load (default as 1), and $p_{0,elc}$ refers to the initial power of electronic load. The parameter variation ranges for electronic load are the shown in Table III.

$$fvl = \begin{cases} \frac{1}{V_{d1}-V_{d2}} \\ \frac{V-V_{d2}}{V_{d1}-V_{d2}} \\ \frac{V_{min}-V_{d2}+frcel \cdot (V-V_{min})}{V_{d1}-V_{d2}} \\ 0 \end{cases} \quad (18)$$

$$p_{elc} = fvl \cdot p_{0,elc}, \quad (19)$$

$$q_{elc} = \tan(\cos^{-1}(pf_{elc})) * p_{elc}. \quad (20)$$

TABLE III
PARAMETER VARIATION RANGE FOR ELECTRONIC LOAD

Parameter	V_{d1}	V_{d2}	pf_{elc}
	[0.60, 0.70]	[0.50, 0.55]	1

F. Identify the Composition of the Composite Load

In a composite load model, different load composition can induce very similar dynamic responses [19], [21]. To conduct load modeling for the WECC CLM, the problem is decomposed into two stages: the first stage finds a load composition that is most likely to represent the true load component fractions at the interested bus; then the load parameters are identified at the second stage. It has been observed in [19] that a different load composition of a big IM and a small IM could have very similar load dynamic responses. This multi-solution phenomenon on load composition is even more common in the WECC CLM due to the multiple IMs in place. Therefore, identifying the most possible load composition can greatly improve the parameter fitting efficiency. Assuming we find N possible load compositions $\mathbf{S}_{1,2,\dots,N}$ for a given dynamic response $\mathbf{P}_{ref}, \mathbf{Q}_{ref}$, for each load composition we define its probability of representing the true load using (21):

$$P(\mathbf{P}_{ref}, \mathbf{Q}_{ref} | \mathbf{S}_n) = \prod_{t=1}^T P[P_{ref,t}, Q_{ref,t} | \mathcal{N}(\mu_{n,t}, \sigma_{n,t})]. \quad (21)$$

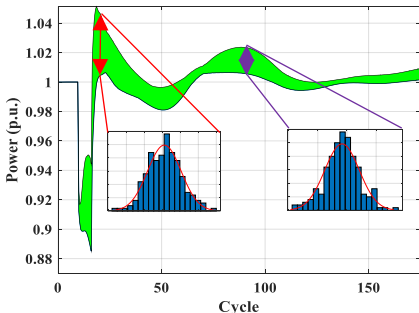


Fig. 2. Dynamic P responses of load models with the same load composition

where $P_{ref,t}$ and $Q_{ref,t}$ are the value of the t^{th} snapshot in \mathbf{P}_{ref} and \mathbf{Q}_{ref} , T refers to the number of snapshots that are being considered, $\mathcal{N}(\mu_{n,t}, \sigma_{n,t})$ represents the Gaussian distribution of the value at the t^{th} snapshot. This distribution is generated from the statistical analysis over massive transient responses of the WECC CLM models with different parameters but the same load composition. $P[P_{ref,t}, Q_{ref,t} | \mathcal{N}(\mu_{n,t}, \sigma_{n,t})]$ indicates the possibility of value $P_{ref,t}$ and $Q_{ref,t}$ existing in distribution $\mathcal{N}(\mu_{n,t}, \sigma_{n,t})$. So $P(\mathbf{P}_{ref}, \mathbf{Q}_{ref} | \mathbf{S}_n)$ indicates the joint probability for the full response. An example is given in Fig. 2 to demonstrate this joint probability calculation for \mathbf{P}_{ref} . In Fig. 2, the green band is generated using 500 random cases under a specific load composition. The value distributions of two snapshots are also presented and assumed to be Gaussian [23]-[24].

G. Monte Carlo-based Parameter Selection

In the last step, the probability of each possible load composition is calculated using (21). Then, from the massive random cases that are used to generate the distributing band as shown in Fig. 2, the set of parameters that best approximates the reference dynamics \mathbf{P}_{ref} and \mathbf{Q}_{ref} is selected as the load modeling result. The fitting accuracy is measured using Root Mean Squared Error (RMSE).

III. DDQN-BASED LOAD COMPOSITION IDENTIFICATION

A. DDQN Agent Training Setup

In double deep Q-learning network, two neural network agents are trained to interact with the environment. Agent A is the prediction network that performs the actions to the environment and updates at each training step, and agent B is the target network which provides a target Q value for agent A's updating while agent B is updated at every C ($C \gg 1$) step. Compared to the regular DQN algorithm, DDQN has better training stability as it avoids the positive bias propagation caused by the max function in Bellman equation [25]. At each state, the environment responds to the taken action. This response is interpreted as reward or penalty. Both agent A and agent B learn the action-reward function $Q(s, a)$ by iteratively updating the Q value following (22), which is fundamentally a Bellman equation. In (22), the $Q^A(s, a)$ and $Q^B(s, a)$ denote the Q functions learned by agent A and agent B; s is the current state; a refers to the current action taken by the agent; α represents the learning rate, which discounts the Q updates to ensure the model doesn't overestimate the reward; r is the immediate reward/penalty by taking action a at state s ; s' is the new state transient from s after action a is taken.

$$Q^A(s, a) = (1 - \alpha)Q^A(s, a) + \alpha \cdot (r + \gamma \cdot \max_{a'} Q^B(s', a)) \quad (22)$$

Function $Q^A(s, a)$ updates at every step following (22), but function $Q^B(s, a)$ updates every C ($C \gg 1$) step. In such a way, the temporal difference (TD) error is created, which serves as the optimization target for the agent, as shown in (23).

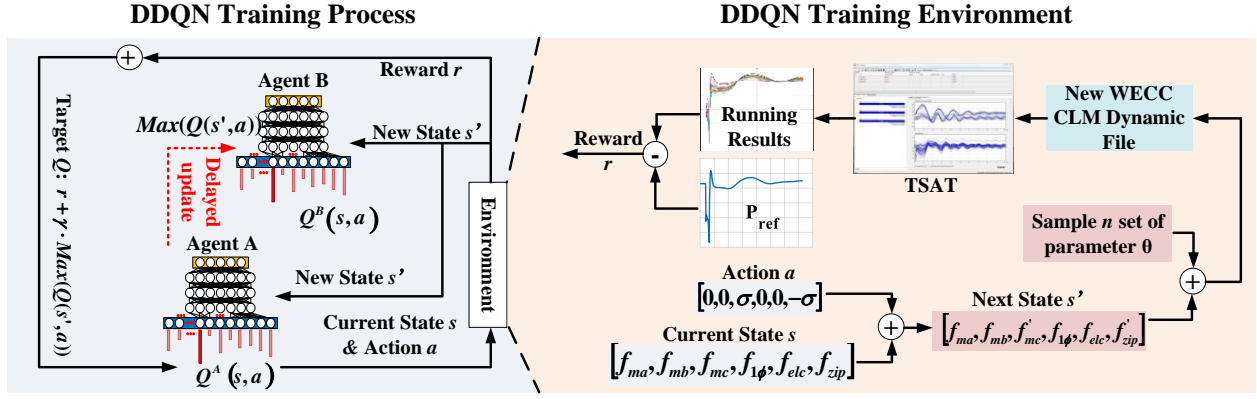


Fig. 3. The DDQN agent training process and training environment introduction

$$\min(L) = \|Q^A(s, a) - r - \gamma \cdot \max Q^B(s', a)\| \quad (23)$$

In this application, the state is defined as the load composition fraction of each load component: $s = [f_{ma}, f_{mb}, f_{mc}, f_{1\phi}, f_{etc}, f_{zip}]$. The summation of s is always one to represent the full load. The actions to be taken by the agents are the pair-wise load fraction modification: $a = [\dots, \rho, \dots, -\rho, \dots]$. ρ is the fraction modification value, which is designed as 0.01 in the case study. Each a_t only has two non-zero elements, which are ρ and $-\rho$. In this case, the summation of s is guaranteed to remain one at each step. Because the WECC CLM contains six load components, the number of actions is $A_6^2 = 30$. The training environment is the IEEE 39-bus system built in the Transient Security Assessment Tool (TSAT) in DSAToolsTM. Fig. 3 shows the DDQN training process and the training environment. Observed from the training environment, when a new state s' is reached, n sets of parameters θ will be sampled, which are then combined with s' to form n dynamic files. The n dynamic files are run in the TSAT in order to calculate the reward.

The pseudo-code for the DDQN agent training is shown in Algorithm I. In the training process the epsilon-greedy searching policy and the memory replay buffer are applied, and the detailed introduction to them can be found from [26], [27], which will not be discussed in this paper.

Algorithm I: DDQN Training for WECC CLM

Input: Reference dynamic responses P_{ref} and Q_{ref} .

Output: Load composition and load parameters

Initialize $\lambda, \gamma, \epsilon, \eta$, NN. A, NN. B and memory buffer M

For i **in** range (number of episode)

$s \leftarrow \text{reset.environment}()$; $\epsilon \leftarrow \epsilon \cdot \eta$; $r_sum \leftarrow 0$; $tik \leftarrow 0$; NN. B \leftarrow NN. A;

While $tik \leq 80$:

If $\text{rand}(1) < \epsilon$:

$a \leftarrow \mathbf{a}(\text{randi}(|30|))$

Else:

$a \leftarrow \mathbf{a}(\text{argmax}(\text{NN. A. predict}(s)))$

End

$s', r \leftarrow \text{execute.TSAT}(s, a)$

If $r > \lambda$

Terminate Episode i .

Else

Step1: $Q^B(s, a) = \text{NN. B. predict}(s, a)$

Step2: $Q^A(s) = \text{NN. A. predict}(s)$

Step3: $Q^A(s)(\text{index}(a \text{ in } \mathbf{a})) = Q^B(s, a) + r$

Sample a batch of transitions D from M

Repeat the Step 1 to Step 3 for each sample in D .

NN. A. fit($[s, s_D], [Q^A(s), Q_D]$)

$M \leftarrow [s, a, s', r]$

$s \leftarrow s'$

$r_sum = r_sum + r$

End

$r_list.append(r_sum)$

End

B. Customized Reward Function

The reward in our application is a negative value that represents the transient P and Q curve fitting losses. The training goal is to minimize the losses. A higher reward means a higher fitting accuracy. At each new state, the dynamic responses are compared with the reference responses to get a reward r , which will be further interpreted into Q value to update the agent A and agent B. However, the classic RMSE loss function cannot properly differentiate the desirable load compositions from the undesirable ones. This phenomenon is further explained later. Therefore, a customized loss function is developed to better capture the dynamic features of the transient curves as shown in (24) and (25):

$$r = -\alpha \cdot r_{RMSE} - \beta \cdot r_{trend} - r_{step} \quad (24)$$

$$r_{trend} = \frac{\sum_{i=1}^n |idx_{min}^i - idx_{min}^{ref}| + |idx_{max}^i - idx_{max}^{ref}|}{K} \quad (25)$$

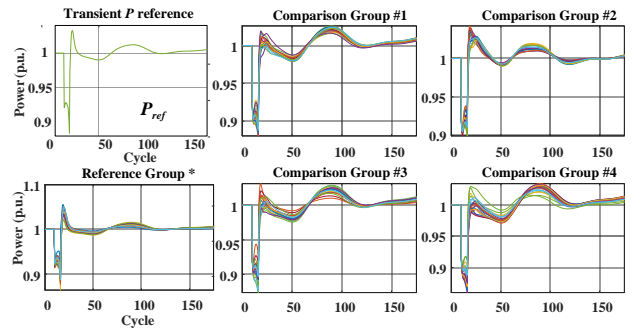


Fig. 4. Loss comparison between reference group and comparison groups

where r_{RMSE} denotes the RMSE between P_{test}, Q_{test} and P_{ref}, Q_{ref} . The regularization term r_{trend} represents the time index mismatch for peak and valley values between P_{test}, Q_{test} and P_{ref}, Q_{ref} . This term explicitly differentiates the desirable

fitting results from others and enforces the similar peak and valley timestamps as $\mathbf{P}_{ref}, \mathbf{Q}_{ref}$. Another regularization term r_{step} is a constant penalty for each step of searching, which facilitates the agent's training speed. By using this customized loss function, a generic fitting accuracy threshold λ can then be set as the episode termination condition. We show some example plots in Fig. 4 to better explain the effects of this customized loss function.

In Fig. 4, the \mathbf{P}_{ref} is a P dynamic response from a WECC CLM, which locates at bus 20 of the IEEE 39-bus system, and a three-phase fault is deployed at bus 6. The plots are normalized based on the power flow solution at steady state; Reference Group* shows multiple \mathbf{P} dynamic responses from multiple WECC CLMs that have the same load composition as the \mathbf{P}_{ref} , but with different load parameters. The other four plots are called the comparison groups, where the transient \mathbf{P} curves are generated by the WECC CLMs with different load compositions. The RMSE and customized loss between the \mathbf{P}_{ref} and these five groups are summarized in Table III. It shows that the RMSEs of the five groups are very close. The boundary between the desirable composition and the undesirable compositions is not clear. In this case, it is difficult to derive a generic threshold λ for the DDQN algorithm that is applicable to all cases. On the contrary, by using the customized loss function, the fitting loss discrepancy between the Reference Group* and other groups are significantly enlarged as shown in Table IV. As a result, a generic and fixed λ can be defined to serve as the termination condition for each episode of training.

TABLE IV
PARAMETER VARIATION RANGE FOR ELECTRONIC LOAD

	Reference Group*	Group 1	Group 2	Group 3	Group 4
RMSE	0.0092	0.0107	0.0135	0.0160	0.0177
Customized Loss	0.0067	0.08348	0.9192	0.7795	0.7578

IV. CASE STUDIES

A. Test Environment

The transient stability test cases shown in this section are conducted in IEEE 39-bus system. In each case study, the base contingency is chosen as a three-phase fault occurred at bus 6, and the load model to be identified locates at bus 20. All the cases are performed using the Transient Security Assessment Tool (TSAT) in DSATools™ developed by Powertech Labs Inc.

B. Case I: Algorithm Test on CLM with ZIP + IM

In Case I, the performance of the proposed algorithm is tested on the conventional ZIP + IM composite load model (CLM). For the DDQN agent, the state vector s indicates the composition of the two load types $s = [s_{zip}, s_{IM}]^T$, ($s_{zip} + s_{IM} = 1$). Since there are only two load components to be identified, the action space only contains two actions, which are $\mathbf{a} = [a_1, a_2]^T = \begin{bmatrix} 0.01 & -0.01 \\ -0.01 & 0.01 \end{bmatrix}$.

The reference load composition is $\mathbf{s}_{ref} = [0.2937, 0.7063]^T$.

The DDQN agent starts to search for possible solutions from a randomly generated load composition [0.4935, 0.5065]. The agent training process is shown in Fig. 5(a). The training reward converges after around 2,000 episodes. The top 3 most possible solutions selected by the trained DDQN agent are listed in Table V and their corresponding P dynamic responses are plotted in Fig. 5(b). All the three solutions found by the agent have very similar dynamic responses with the actual load model.

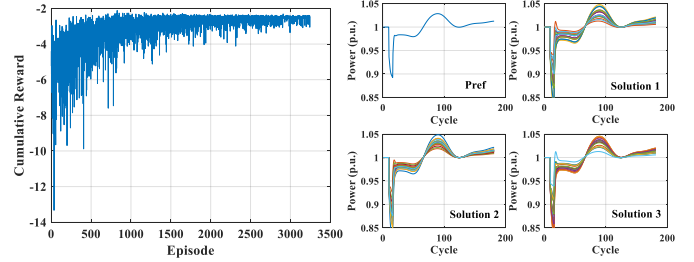


Fig. 5. (a) DQN training process (b) Reference P curve and possible solutions

TABLE V
CANDIDATE LOAD COMPOSITION

	True	Solution 1	Solution 2	Solution 3
ZIP	0.2937	0.2835	0.2935	0.3035
IM	0.7063	0.7165	0.7065	0.6965
$P(\mathbf{P}_{ref} \mathbf{s}^N)$		3.66e-20	1.08e-15	4.33e-19

The possibilities of the three solutions are calculated following the method introduced in Section II and the results are listed in Table V. Among the three solutions, solution 2 has the highest probabilities. Therefore, it is selected as the load composition identification solution: $\mathbf{s} = [0.2935, 0.7065]^T$.

Based on the solution, 500 Monte Carlo samplings are conducted on the load parameters. The one set of parameters, yielding the lowest dynamic response reconstruction error, is selected as the identified load parameters. The reference load parameters and the identified load parameters are shown in Table VI. Except P_{1C} and P_{2C} , all the other parameters are well fitted. The P and Q transient dynamic response comparisons between the reference model and the identified model are shown in Fig. 6. The active power P fitting RMSE is 0.0692% and the reactive power Q fitting RMSE is 0.68%.

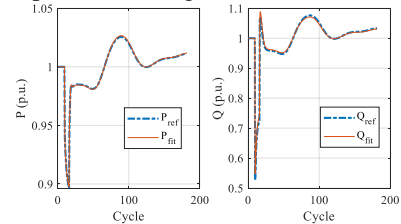


Fig. 6. Dynamic responses comparison between the reference load and the fitted load.

TABLE VI
CANDIDATE LOAD COMPOSITION

	R_s	L_s	L_p	L_{pp}	T_{p0}	T_{pp0}
Ref	0.0314	1.9013	0.1228	0.1040	0.0950	0.0021
Fit	0.0327	1.8558	0.1328	0.1032	0.0938	0.0021
	H	$Etrq$	P_{1C}	P_{2C}	Q_{1C}	Q_{2C}
Ref	0.1000	0	0.0316	0.6947	-0.4769	1.4769
Fit	0.1030	0	0.0274	0.2287	-0.4477	1.4477

C. Case II: Algorithm Test on WECC CLM

In this case, the proposed DDQN-based load composition identification strategy is applied to the WECC CLM. Compared with Case I, the number of load component in the WECC CLM increases from two to six. Therefore, the state vector size turns into 6×1 . The number of actions can be taken by the agent also increases to $A_6^2=30$. The action step size is 0.01, which means the load composition changes 1% at each step. This case study aims to demonstrate that the proposed method is scalable to larger load models.

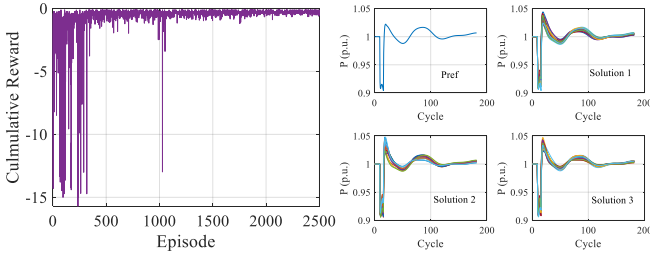


Fig. 7. (a) DDQN training process (b) Reference P curve and possible solutions

The reference load composition is $\mathbf{s}_{WECC} = [0.3637, 0.1430, 0.0914, 0.1526, 0.1088, 0.1405]^T$. The training starting state is defined as $[1/6, 1/6, 1/6, 1/6, 1/6, 1/6]^T$. The training reward converges after 1,100 episodes as shown in Fig. 7 (a). The top three most possible solutions given by the agent are listed in Table VII and their corresponding P dynamic responses are plotted in Fig. 7 (b).

	True	Solution 1	Solution 2	Solution 3
IM_A	0.3637	0.1667	0.1867	0.2067
IM_B	0.1430	0.1667	0.1667	0.1667
IM_C	0.0914	0.1667	0.1667	0.1667
IM_lp	0.1526	0.1667	0.1867	0.1867
ELC	0.1088	0.2067	0.1667	0.1667
ZIP	0.1405	0.1267	0.1267	0.1067
Dynamic	0.7507	0.6667	0.7067	0.7266
Static	0.2493	0.3333	0.2933	0.2734
$P(P_{ref} S^N)$		$3.44e-15$	$1.48e-15$	$6.98e-16$

Unlike the conventional CLM with only one IM, the WECC CLM has three IMs and one single-phase IM; therefore, the transient dynamics between each load component has more mutual interference. For each transient event, there exist multiple load composition solutions with very similar transient dynamics [21]. As shown in Table VII, the top three most possible solutions are listed. For those three solutions, the fraction distribution among dynamic loads and static loads are close to the reference load model. During the training process, the DQN agent gradually learns to choose solutions with higher fitting possibilities $P(P_{ref}|S^N)$; in other words, a more stable solution emerges so that each episode is terminated with fewer exploration steps. Fig. 8 shows the agent's selection migration among the top three possible solutions: from episode 1901 to episode 2100, solution 1 is not found by the agent; solution 3 is more frequently selected than solution 2. After another 200 episodes, solution 1 is still not found; the selection frequency of solution 2 quickly exceeds solution 3 due to its higher fitting

possibility. During the final 200 episodes, solution 1 is found by the agent, its selection frequency quickly exceeds solution 2 and solution 3; the selection frequency of solution 2 increases by five times and the selection frequency of solution 3 does not increase in the last 200 episodes. This selection migration shows that the agent keeps pursuing a more stable (higher fitting possibility) solution during the training process, so that it can earn a high reward more frequently.

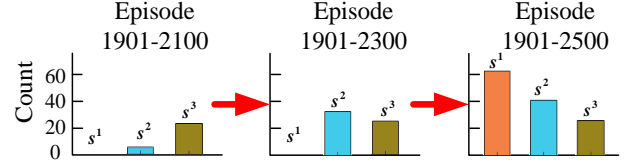


Fig. 8. Occurrence of solutions 1-3 at the last 600 episodes

According to the possibility rank, solution 1 is chosen as the load composition solution. Based on this result, 500 Monte-Carlo samplings are conducted to select a set of parameters that best match with the reference P and Q. The best fitting result is shown in Fig. 9. Due to space limitation, the parameters of the reference load and identified load are not presented.

Noted, the initial state is selected assuming no prior information about the load composition. When there is previous load statistics, a better initial state can be derived.

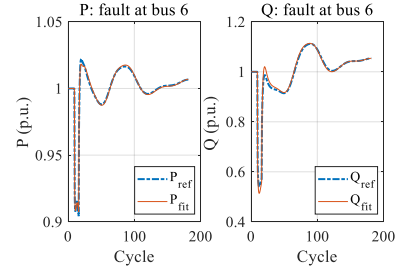


Fig. 9. Dynamic responses comparison between the reference load and the fitted load.

D. Case III: Model Robustness Tests

One of the most important reasons for load modeling is to have a consistent load representation that can closely reflect the real transient dynamics under different contingencies. For that purpose, another two groups of robustness tests are simulated. In the first group, the fault location is changed from bus 1 all the way up to bus 39. In the second group, the fault type is modified from three-phase fault to single-phase-to-ground fault and two-phase-to-ground fault.

The results of the first group of tests show that when the fault occurs at other buses, the P , Q transient curves of the identified load model still fit the true transient curves very well. Fig. 10 shows the P , Q transient examples for faults that occur at bus 14 and bus 29, respectively. In this group of tests, the active power P 's fitting RMSE has a mean value of 0.0995% ($0.0255\% \leq RMSE_P \leq 0.2124\%$). For reactive power Q , the mean fitting RMSE is 0.7852% ($0.2374\% \leq RMSE_Q \leq 1.5939\%$). The high dynamic fitting accuracy achieved by the fitted load model demonstrates the proposed load modeling method's robustness towards faults that occur at

different locations.

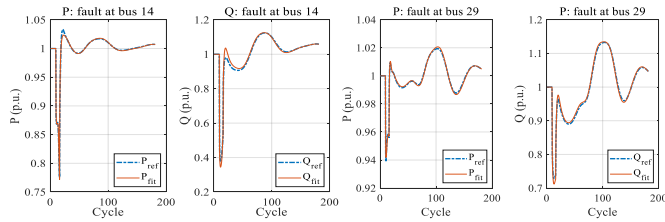


Fig. 10. P and Q fitting comparisons when fault occurs at different buses.

The results of the second group of tests show that the identified load model can capture the transient behaviors of the reference load model under different fault types. Fig. 9 shows the P , Q fitting curves of our identified load model when single-phase-to-ground fault and double-phase-to-ground fault occur at bus 6. The same test at other buses are also conducted. In summary, the mean P fitting RMSE is 0.0714% ($0.0236\% \leq RMSE_P \leq 0.1447\%$); the mean Q fitting RMSE is 0.7216% ($0.2111\% \leq RMSE_Q \leq 1.3372\%$). This test demonstrates the robustness of the proposed load modeling method towards different fault types. The case study also proves the scalability of the method to larger load models.

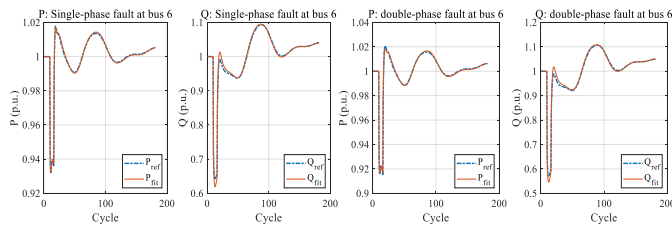


Fig. 11. P and Q fitting comparisons for single-phase to ground fault and double-phase to ground fault.

V. CONCLUSIONS

In this paper, a two-stage load modeling and identification method for WECC CLM is proposed. The first stage determines the load composition, and the second stage identifies the load parameters. This method offers the following contributions and advantages: it requires very limited prior knowledge towards hard-to-obtain and constantly updating load structure statistics. It is also scalable, from conventional composite load model such as ZIP + IM to complex load models such as the WECC CLM, or even more complex load models when additional load components are added. In addition, the identified load model using the proposed method is robust to different fault types and faults that occur at different locations. Furthermore, unlike common data-hungry methods that rely on a large number of disturbances data to calibrate, the proposed method only requires a set of reference dynamic responses, which is much more convenient to obtain.

REFERENCES

- [1] P. Kundur, *Power System Stability and Control*. New York: McGrawHill, 1993.
- [2] J. V. Milanovic, K. Yamashita, S. Martínez Villanueva, S. Ž. Djokic and L. M. Korunović, "International industry practice on power system load modeling," *IEEE Transactions on Power Systems*, vol. 28, no. 3, pp. 3038-3046, Aug. 2013.
- [3] Y. Li, H.-D. Chiang, B.-K. Choi, Y.-T. Chen, D.-H. Huang, and M.G. Lauby, "Load models for modeling dynamic behaviors of reactive loads: Evaluation and comparison," *International Journal of Electrical Power & Energy Systems*, vol. 30, no. 9, pp. 497-503, 2008.
- [4] M. Jin, H. Renmu, and D. J. Hill, "Load modeling by finding support vectors of load data from field measurements," *IEEE Transactions on Power Systems*, vol. 21, no. 2, pp. 726-735, May 2006.
- [5] C. Wang, Z. Wang, J. Wang, and D. Zhao, "Robust time-varying parameter identification for composite load modelin," *IEEE Transactions on Smart Grid*, vol. 10, no. 1, pp. 967-979, Jan. 2019.
- [6] D. Han, J. Ma, R. He et al., "A real application of measurement-based load modeling in large-scale power grids and its validation," *IEEE Transactions on Power Systems*, vol. 24, no. 4, pp. 1756-1764, Nov. 2009.
- [7] P. Ju et al., "Composite load models based on field measurements and their applications in dynamic analysis," *IET Generation, Transmission & Distribution*, vol. 1, no. 5, pp. 724-730, Sep. 2007.
- [8] A. Borden and B. Lesieutre, "Model validation: FIDVR event," Univ. of Wisconsin-Madison, Madison, WI, USA, Tech. Rep., 2009.
- [9] D. Kosterev et al., "Load modeling in power system studies: WECC progress update," in *2008 IEEE Power and Energy Society General Meeting - Conversion and Delivery of Electrical Energy in the 21st Century*, Pittsburgh, PA, 2008, pp. 1-8.
- [10] NERC, "Dynamic Load Modeling," Nov. 2016.
- [11] Siemens Industry, Inc, software manual: "PSS®E 33.10, MODEL LIBRARY," Apr. 2017.
- [12] Q. Huang, R. Huang, B. J. Palmer, Y. Liu, S. Jin, et al., "A generic modeling and development approach for WECC composite load model," *Electric Power Systems Research*, vol. 172, pp 1-10, 2019.
- [13] A. Gaikwad, P. Markham, and P. Pourbeik, "Implementation of the WECC composite load model for utilities using the component-based modeling approach," in *2016 IEEE/PES Transmission and Distribution Conference and Exposition (T&D)*, Dallas, TX, 2016, pp. 1-5.
- [14] P. Etingov, "Load model data tool (LMDT)," <https://svn.pnl.gov/LoadTool>.
- [15] Jae-Kyeong Kim et al., "Fast and reliable estimation of composite load model parameters using analytical similarity of parameter sensitivity," in *2016 IEEE Power and Energy Society General Meeting (PESGM)*, Boston, MA, 2016, pp. 1-1.
- [16] S. Son et al., "Improvement of composite load modeling based on parameter sensitivity and dependency analyses," *IEEE Trans. Power Syst.*, vol. 29, no. 1, pp. 242-250, Jan. 2014.
- [17] K. Zhang, H. Zhu, and S. Guo, "Dependency analysis and improved parameter estimation for dynamic composite load modeling," *IEEE Transactions on Power Systems*, vol. 32, no. 4, pp. 3287-3297, Jul. 2017.
- [18] Western Electricity Coordinating Council, Technical Reference Document: "WECC Composite Load Model Specifications" Jan. 2015, <https://www.wecc.org/>
- [19] S. Guo, T. J. Overbye, "Parameter estimation of a complex load model using phasor measurements," in *Proc. Power Energy Conf.*, Illinois, Feb. 2012, pp. 1-6.
- [20] NERC Technical Reference Document: "A Look into load modeling: The composite load model." Sep. 2015, <https://gig.lbl.gov/sites/all/files/6b-quint-composite-load-model-data.pdf>
- [21] B. K. Choi, H. D. Chiang, "Multiple solutions and plateau phenomenon in measurement-based load model development: Issues and suggestions," *IEEE Trans. Power Syst.*, vol. 24, no. 2, pp. 824-831, May 2009.
- [22] Pacific Northwest National Laboratory, Technical Reference Document: "Composite load model evaluation," Sep. 2015.
- [23] P. Chen, B. Bak-Jensen, and Z. Chen, "Probabilistic load models for simulating the impact of load management," in *2009 IEEE Power & Energy Society General Meeting*, Calgary, AB, 2009, pp. 1-8.
- [24] A. Seppala, "Statistical distribution of customer load profiles," in *Proc. 1995 International Conference on Energy Management and Power Delivery EMPD '95*, Singapore, 1995, pp. 696-701 vol.2.
- [25] H. V. Hasselt, A. Guez, and D. Silver, "Deep reinforcement learning with double Q-learning," arXiv:1509.06461, 2016.
- [26] I. Durugkar and P. Stone, "TD learning with constrained gradients," in *Proc. of the Deep Reinforcement Learning Symposium (NIPS 2017)*, Long Beach, CA, USA December 2017.
- [27] R. Liu and J. Zou, "The effects of memory replay in reinforcement learning," *The ICML 2017 Workshop on Principled Approaches to Deep Learning*, Sydney, Australia, 2017. <https://www.padl.ws/papers/Paper%2018.pdf>. Accessed 2019.